Hematocrit and flow rate regulate the adhesion of platelets to von Willebrand factor

Hsieh Chen, Jennifer I. Angerer, Marina Napoleone, Armin J. Reininger, Stefan W. Schneider, Achim Wixforth, Matthias F. Schneider, Alfredo Alexander-Katz

Hematocrit and flow rate regulate the adhesion of platelets to von Willebrand factor

Hsieh Chen, Jennifer I. Angerer, Marina Napoleone, et al.

View Online   Export Citation   CrossMark

ARTICLES YOU MAY BE INTERESTED IN

Hematocrit and flow rate regulate the adhesion of platelets to von Willebrand factor

Hsieh Chen,[1] Jennifer I. Angerer,[2,3] Marina Napoleone,[3]
Armin J. Reininger,[4] Stefan W. Schneider,[5] Achim Wixforth,[2]
Matthias F. Schneider,[6] and Alfredo Alexander-Katz[1,a)]

[1]*Department of Materials Science and Engineering, Massachusetts Institute of Technology, Cambridge, Massachusetts 02138, USA*
[2]*Experimental Physics I, Biological Physics Group, University of Augsburg, 86159 Augsburg, Germany*
[3]*Department of Transfusion Medicine/Haemostaseology, University Clinic Munich, LMU, 80337 Munich, Germany*
[4]*Baxter Innovations GmbH, Vienna, Austria*
[5]*Department of Dermatology, Venereology, and Allergology, Experimental Dermatology, Medical Faculty Mannheim, Heidelberg Ruprecht-Karls-University, 68167 Mannheim, Germany*
[6]*Department of Mechanical Engineering, Boston University, Boston, Massachusetts 02215, USA*

Primary hemostasis and blood clotting is known to be influenced by the red blood cell volume fraction (hematocrit) in blood. Depressed or elevated levels of red blood cells can lead to vascular perfusion problems ranging from bleeding to thrombus formation. The early stage of hemostasis and thus blood clotting in all vessel sections from the arterial to the venous system involves the adhesion of platelets to von Willebrand factor. Here we present experimental and theoretical results showing that the adhesion probability of platelets to von Willebrand factor is strongly and nonlinearly dependent on hematocrit and flow rate. Interestingly, the actual binding forces are not markedly different, which suggest that the origin of such behavior is in the distribution of platelets. Using hydrodynamic simulations of a simple model, we explicitly show that the higher the hematocrit and the flow rate, the larger the amount of platelets residing close to the wall. Our simulation results, which are in excellent agreement with the experimental observations, explain why such phenomena occur. We believe that the nonhomogeneous red blood cell distribution as well as the shear dependent hydrodynamic interaction is key for the accumulation of platelets on the vessel wall. The work we present here is an important step forward from our earlier work on single molecules and extends into the collective cellular behavior of whole blood. It sheds new light on the correlation between hematocrit and the initial steps in hemostasis and thrombosis, and outlines advances for the treatment of vascular diseases associated with high levels of red blood cells. These results are not only highly relevant for the field of hemostasis and the physics of blood clotting but are also of powerful impact in applied science most obviously in drug delivery and colloidal science. © *2013 AIP Publishing LLC*. [http://dx.doi.org/10.1063/1.4833975]

INTRODUCTION

The formation of a clot in the arterial vasculature is dependent on the adhesion of von Willebrand factor (vWF) to the injured endothelium and the subsequent adhesion of platelets to vWF.[1–5] This process is known as primary hemostasis and leads to the formation of the cellular

---

a)E-mail: aalexand@mit.edu

plug that serves as a scaffold for the assembly of clotting factors ultimately leading to the stable fibrin clot.[6,7] There are many factors that can affect this process such as mutations or reduced levels of "active" vWF, normally referred to as von Willebrand Disease,[8–10] as well as abnormal counts of platelets.[11,12] Deficiencies of vWF-degrading protease (ADAMTS-13) lead to multiple vWF-platelet rich plugs that usually are fatal to the patient—the disease is known as Thrombotic Thrombocytopenic Purpura.[13,14] However, there are other conditions that strongly affect the formation of thrombi that are not directly related to the cellular and plasmatic constituents of clots *per se*. One of the most important factors, which regulate the correct plug formation and thereby the clotting process, is the volume fraction of red blood cells (RBCs), the so-called hematocrit. It is known that elevated or depressed levels of the hematocrit can cause severe vascular disorders.[15] In particular, higher than normal values as found in essential thrombocythemia can lead to thrombosis and increase the risks of stroke or heart attack, while lower than normal levels can lead to bleeding.

Previous studies have found that platelets or small colloids in the presence of RBCs accumulate near the walls of the blood vessels,[16–21] and the degree of accumulation is dependent on the wall shear rate and the hematocrit. However, there remain some important questions, such as how the accumulation of platelets affects their binding to vWF.[5,22–24] Here, we present experimental results on the adhesion of platelets to vWF carpets by directly imaging the adhesion zone next to the wall, which is only a few nanometers thick, using Reflection Interference Contrast Microscopy (RICM) under flow.[25,26] Note that the platelet adhesion to vWF is very different from its adhesion to other thrombogenic surfaces such as fibrinogen or endothelium.[27–30] As observed in previous studies, the vWF/platelet GP1b-α interaction is characterized by a fast association and disassociation rate, resulting in platelet translocation on vWF.[22,23] On the other hand, the platelet adhesion to endothelium is a slow yet firm process in which the platelets are usually immobilized after attachment. The reaction kinetics has a dramatic effect on platelet adhesion. In the perfusion experiments, the platelet adhesion to vWF usually saturates in the first minute, while the platelet adhesion to endothelium may continuously grow after 100 min.[31] Our experiments clearly show that platelet adherence to vWF also has a strong dependence on the hematocrit and the flow rate, increasing drastically if both or either of these control parameters is increased. Interestingly, we did not observe any significant change in the adhesion area, indicating that the adhesion energy remains unchanged and that this phenomenon must be due primarily to the higher concentration of platelets. To understand this behavior, we performed Lattice Boltzmann (LB) simulations[32,33] of a mixture of colloids with sizes and concentrations reflecting those of RBCs and platelets from our experiments. The simulations show clearly the formation of a platelet-rich region near the wall.

There have been tremendous studies on the lateral migration of particles in flow.[34–41] The redistribution of platelets near walls in flowing blood is known as platelet margination.[42–47] Although it is well observed in experiments[16–21] and computer simulations,[45–49] the origin of the margination is still controversial.[42–52] For example, Kumar and Graham have attributed the phenomenon to heterogeneous collisions between stiff and floppy colloids.[42–44] Zhao and Shaqfeh have described the expulsion of platelets by the velocity fluctuations in the core cellular flow toward the cell-depleted layer near the wall.[45,46] Tokarev and coworkers have suggested the finite platelet size to be responsible for the margination.[50] On the other hand, Eckstein and coworkers have established a phenomenological drift-diffusion model to describe the platelet motion in blood flow.[51,52] Through empirically choosing the drift functions, the authors were able to reconstruct the experimental observations. Here we adopt the drift-diffusion model as the basis for our theoretical approach. The drift functions are derived directly from the distributions of the RBC-like colloids in our LB simulations. Our theoretical approach is tested with stochastic differential equation (SDE) simulations.[49,51] The platelet distributions from the SDE simulations agree particularly well with the explicit LB simulations, as well as the experiments. This combination of experimental and theoretical efforts is an important step forward towards as deeper understanding of the effects of abnormal red blood cell concentrations,[15] and gives insight into separation processes in mixtures of colloids that can find uses in separations or coatings.[53–55]

MATERIALS AND METHODS

Preparation of blood samples

Venous blood (10 ml) from healthy consenting donors was collected in test tubes containing the anticoagulant acid citrate dextrose (0.106 M trisodium citrate), the thrombin inhibitor H-D-Phe-Pro-Arg chloromethyl ketone (PPACK; 46 μM; Bachem, Bubendorf, Switzerland), prostaglandin E1 (PGE1; 0.35 μl/ml; Sigma), aggrastat concentrate (0.25 μg/ml; MSD Sharp & Dohme GmbH, Haar, Germany), and apyrase grade 7 (1.3 ATPase U/ml; Sigma). The blood samples were centrifuged at 170 g for 15 min. The platelet rich plasma (PRP) was further centrifuged at 1083 g for 15 min to obtain platelet plasma (PPP). The platelet count in the final suspension was adjusted to 200 000/μl, and the hematocrit was adjusted to around 20%, 40%, and 60%.[24]

Microscopy and image acquiring

RICM (Axioskop 2 plus; Zeiss, Germany) was performed using a plan neofluoar antiflex objective (63×, oil immersion, N.A. = 1.6, Zeiss, Germany) and a 50-W mercury lamp for illumination. Interference colors were obtained in grey scale. All experiments were recorded on DVD using a CCD camera (BC-71, AVT Horn, Aalen, Germany) and DVD recorder (LQ-MD800 Medical Grade DVD Video Recorder, Panasonic, Germany) at the acquisition rate of 25 frames s^{-1}. Image analysis was performed off-line using Metamorph (Universal Imaging, West Chester, PA) and Matrox (Imaging, Dorval, Quebec, Canada).

Lattice Boltzmann simulations

The simulations are performed on three-dimensional grids with periodic boundary conditions in the x and y directions, and a no-slip boundary condition in the z direction. A uniform pressure is applied in the $+x$ direction, obtaining a planar Poiseuille flow. A grid spacing $\Delta x = 2 \mu$m and a time step $\Delta t = 2 \mu$s are used as the Lattice Boltzmann parameters along with the kinematic viscosity $\nu \approx 10^{-6}$ m^2/s. The channel height is chosen to match the experiments $H/\Delta x = 64$. The wall shear rate $\dot{\gamma}_w \Delta t$ is measured directly from the fluid profile on wall regions. RBC-like and platelet-like colloids are simulated with impenetrable spheres with radius $R/\Delta x = 2.5$ and $r/\Delta x = 0.5$ respectively. For more details, we refer the readers to Refs. [32], [33], [56], and [57].

RESULTS AND DISCUSSION

Real-time visualization of platelet adhesion

Perfusion experiments were performed at 37 °C using immobilized multimeric vWF (Haemate HS250; final concentration: 100 μg/ml; CSL Behring GmbH, Wien, Austria) coated onto a glass cover slip as a substrate and assembled with parallel plates to form an optical accessible rectangular flow chamber (dimension: 30 mm × 3 mm × 127 μm). A syringe pump (Harvard Apparatus, Boston, MA) was used to aspirate anticoagulated reconstructed blood containing activation blocked platelets through the chamber mounted on the stage of an upright reflection interference contrast microscope (see Materials and Methods for blood preparation and imaging techniques). At wall shear rates $\dot{\gamma}_w$ ranging from 400 s^{-1} to 10 000 s^{-1} and hematocrit ϕ_{RBC} from 20% to 60%, platelets always arrested from flowing blood onto immobilized vWF multimers via their formation of discrete adhesion points (DAPs)[5,24] (except for $\phi_{RBC} = 20\%$ at $\dot{\gamma}_w = 400$ s^{-1}, where the platelet lateral diffusion was too slow for them to reach the wall). RICM[25,26] images of activation blocked platelets adhering to vWF-coated surfaces at $\dot{\gamma}_w = 10 000$ s^{-1} for different ϕ_{RBC} are presented in Fig. 1. In the images, each arrested platelet was recognized as multiple black spots (interpreted as DAPs; see Fig. 1(a) Inset) within a surrounding light gray-white membrane area (indicated by black arrows in Fig. 1). Previous studies have suggested that the DAPs were the points of shortest distance in the range of 7 nm between platelet membrane and immobilized vWF, possibly bridged by the GPIb-α receptor protruding
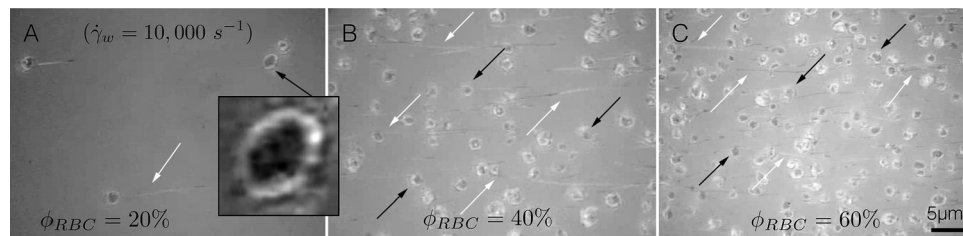
FIG. 1. RICM images of activation-blocked platelets in reconstructed blood samples flowing over vWF-coated surface at wall shear rate $\dot{\gamma}_w = 10\,000\,\text{s}^{-1}$ with hematocrit ϕ_{RBC} (a) 20%, (b) 40%, and (c) 60%. Inset in (a): Single transiently adherent platelet with multiple DAPs.

from the platelet surface to vWF A1 domain.[24] Furthermore, it was observed that tethers are pulled out of the platelet membrane, yielding tube-shaped platelet fragments (indicated by white arrows in Fig. 1). These fragments translocated independently or detached completely from the vWF surface and formed isolated tethers as previously observed by Reininger and coworkers.[24,58] This phenomenon appears to occur when the force moving the platelet forward is matched by the adhesive strength of the DAPs and tether pulling and detachment is a means to protect the platelet from overall rupture.

The RICM technique, which allows to study whole blood without the need of fluorescent or other labels, resolves the contact area between cell membrane and adhesive surface and indicates the separation distance through interference colors.[25,26] The label-free technique enables a high time resolution and allows therefore to study the adhesion dynamics under flow. Assuming a uniform cell membrane, the adhesion area of an arrested platelet is proportional to the total adhesion energy. To obtain the complete picture of the adhesion behavior of platelets, we analyzed the distribution of the adhesion areas and their averages as shown in Fig. 2(a). For all the investigated data, the adhesion areas were homogeneously distributed in the range between 1 and 11 μm^2. At $\dot{\gamma}_w = 1,500\,\text{s}^{-1}$, the average areas (which are 5.8 μm^2 for $\phi_{RBC} = 20\%$, 4.7 μm^2 for $\phi_{RBC} = 40\%$, and 4.6 μm^2 for $\phi_{RBC} = 60\%$) are comparable for all examined hematocrit levels. However, at $\dot{\gamma}_w = 10\,000\,\text{s}^{-1}$, the average areas (which are 6.2 μm^2 for $\phi_{RBC} = 20\%$, 4.9 μm^2 for $\phi_{RBC} = 40\%$, and 3.9 μm^2 for $\phi_{RBC} = 60\%$) decrease with increasing hematocrit (Fig. 2(b)), indicating a decline of adhesion energy for the arrested platelets with increasing hematocrit. The decrease of average adhesion area with increasing hematocrit may be caused by the increased suspension viscosity near walls from increased red blood cell concentrations as well as the near-wall excess of platelets, which increase the hydrodynamic drag force on walls to detach the arrested platelets.

Number of adherent platelets regulated by hematocrit and flow rate

After investigating the platelet adhesion areas, we now discuss the number of platelets adhering to vWF that is observed to be largely dependent on hematocrit and flow rate. In Figs. 1(a) to 1(c), we present the RICM images from the flow experiments at $\dot{\gamma}_w = 10\,000\,\text{s}^{-1}$ with different hematocrit. As can be seen clearly, high hematocrit largely increased the number of adherent platelets. Figure 3 depicts the average number of platelets arrested onto the vWF-coated surface as obtained from the RICM image analysis. The platelet counts are collected at least 1 min after perfusion to ensure the surface platelet coverage has reached its equilibrium value.[22] In general, the platelet adhesion count increased with higher hematocrit and wall shear rate. At wall shear rate $\dot{\gamma}_w = 1500\,\text{s}^{-1}$, the adhesion count for 40% hematocrit was slightly higher than that for 60% hematocrit; however, the difference was within the experimental errors. In addition, it was observed that for all ϕ_{RBC} the platelet adhesion count increased drastically at the range $\dot{\gamma}_w < 4000\,\text{s}^{-1}$, while largely saturated at $\dot{\gamma}_w > 4000\,\text{s}^{-1}$.

The observed results may look surprising at first glance since the highest adhesion count occurred at the highest $\dot{\gamma}_w$ and ϕ_{RBC} where the lowest adhesion energy is assumed (smallest average adhesion area), while at lower $\dot{\gamma}_w$ and ϕ_{RBC} where higher adhesion energy is expected
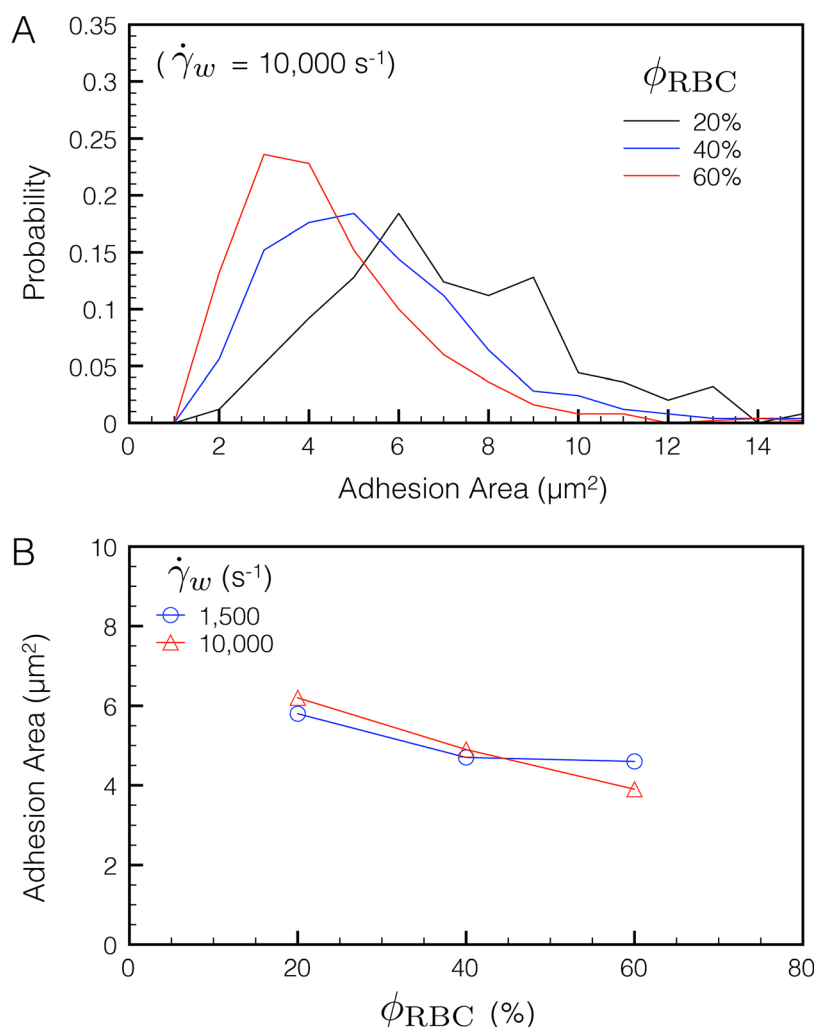
FIG. 2. (A) Distributions of adhesion areas of platelets arrested onto vWF-coated surface observed from RICM images at wall shear rate $\dot{\gamma}_w = 10\,000\,\mathrm{s}^{-1}$ with different hematocrit ϕ_{RBC}. (B) Averaged platelet adhesion areas as a function of ϕ_{RBC} for $\dot{\gamma}_w = 1500$ and $10\,000\,\mathrm{s}^{-1}$. (Contact area $+/- 0.25\,\mu m^2$.)

(larger average adhesion area) we observed less adhesion. To resolve this discrepancy, it is necessary to consider the overall platelet concentration distribution across the flow channel. In fact, it has been known for decades that for flowing blood in a channel, there exists large near-wall accumulation of platelets.[16–21] Nevertheless, due to the difficulties of the experiments, the precise distribution of both cells (platelets and RBCs) across the channel has not been measured until very recently.[59–62]

Lattice Boltzmann simulations of colloidal mixtures

To gain more insight into the distribution of cells in flowing blood, we performed LB simulations[32,33] of a mixture of colloids with sizes and concentrations reflecting those of RBCs and platelets from our experiments. Simulations of flowing blood cell mixtures have been performed with various models including rigid[63–65] or deformable particles.[46,47,66] Deformable RBC is necessary in order to resolve the crowed traffic in high concentration regions, especially the region near flow axis. However, to our knowledge, these deformable simulation model are limited to low shear rates ($\dot{\gamma}_w < 1000\,\mathrm{s}^{-1}$) and short times that are not appropriate for our specific study.[47] On the other hand, in the near-wall region where the local shear rate is the highest, the cells can tank-tread with uniform inclination angle and rigid-like interactions.[46,49,67–69] As a
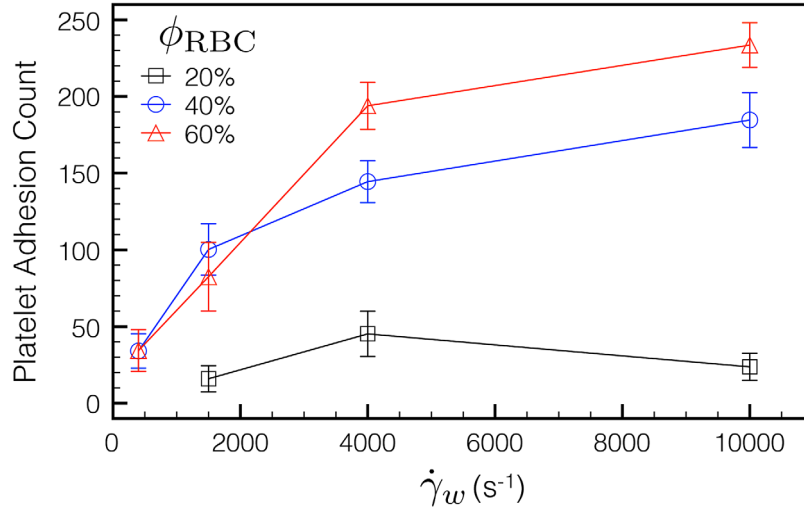
FIG. 3. Mean platelet adhesion count observed from RICM images at different wall shear rate $\dot{\gamma}_w$ and hematocrit ϕ_{RBC}.

result, we believe the hard-sphere assumption is enough to study the flow-induced platelet margination observed in our experiments. Figure 4(a) shows the representative snapshot of the simulations at steady state. It is clearly seen that the platelet-like colloids (smaller blue beads) accumulate to the walls, while RBC-like colloids (larger red beads) accumulate in the center. Fig. 4(b) shows the near-wall number density of platelet-like colloids n_w/n_0 as a function of wall shear rate $\dot{\gamma}_w \Delta t$ with volume fraction of RBC-like colloids $\phi_0 = 10\%$, 20%, and 40%, where n_0 is the bulk number density of platelet-like colloids (which occupy less than 1% of the total volume) and Δt is the LB time step which was set as $\Delta t = 2\,\mu s$. We use $n_0 = 0.00143/\Delta x^3 \approx 180\,000/\mu l$ that matches to our experimental conditions. Also we selected the above concentrations because they match the viscosity of higher contents of RBCs. The near-wall colloids are identified such that $|z_{colloid} - z_{wall}|/\Delta x < 2$, where $z_{colloid}$ and z_{wall} are the height of colloids and walls respectively, and $\Delta x = 2\,\mu m$ is the LB unit length. As shown, n_w/n_0 increases with increasing ϕ_0 and $\dot{\gamma}_w \Delta t$, which is in excellent agreement with the experimental observations (Fig. 3(a)). Furthermore, it is observed that n_w/n_0 increases more rapidly at $\dot{\gamma}_w \Delta t < 0.01$ ($\dot{\gamma}_w < 5000\,\mathrm{s}^{-1}$) and saturates at $\dot{\gamma}_w \Delta t > 0.01$ ($\dot{\gamma}_w > 5000\,\mathrm{s}^{-1}$), again agreeing excellently well with the experiments.

Figure 5 shows the distribution of both colloids across the simulation channel at selected $\dot{\gamma}_w \Delta t$ and ϕ_0. As shown, the distribution of platelet-like colloids n/n_0 (blue curve) is largely regulated by the distribution of RBC-like colloids ϕ (red curve) and is concentrated to the wall regions. Note that the exact distribution of ϕ deviates from other simulations of similar systems[45,46,49] since the deformability of RBCs is not explicitly included. However, it was observed by Zhao and Shaqfeh that the dynamics of RBCs becomes largely independent of deformability when the capillary number $Ca > 1$ ($\dot{\gamma}_w > 2000\,\mathrm{s}^{-1}$) in the specific case of RBCs) as the RBC shape elongation saturates.[45,46] In Figure 5, the strong oscillation of the distribution of the RBC-like colloids at $\phi_0 = 40\%$ comes from the hard-sphere assumption and the presence of solid walls.[70–72] Nevertheless, it is expected that such oscillation should be less obvious in true blood with finite deformability of the blood cells and the vessel walls. Lastly, at $\dot{\gamma}_w \Delta t \approx 0.02$ and $\phi_0 = 10\%$, we see that ϕ accumulates off center compared to other simulation conditions where ϕ all accumulates in the center, which is caused by the dominant hydrodynamic pinching effect at high flow rate for very dilute suspensions.[73]

Solving lateral migration of platelets with drift and diffusion model

Solving the lateral distribution of platelets or platelet size colloids in flowing blood has been an active research area because of its immediate relevance to thrombus formation[30,31,74–78]
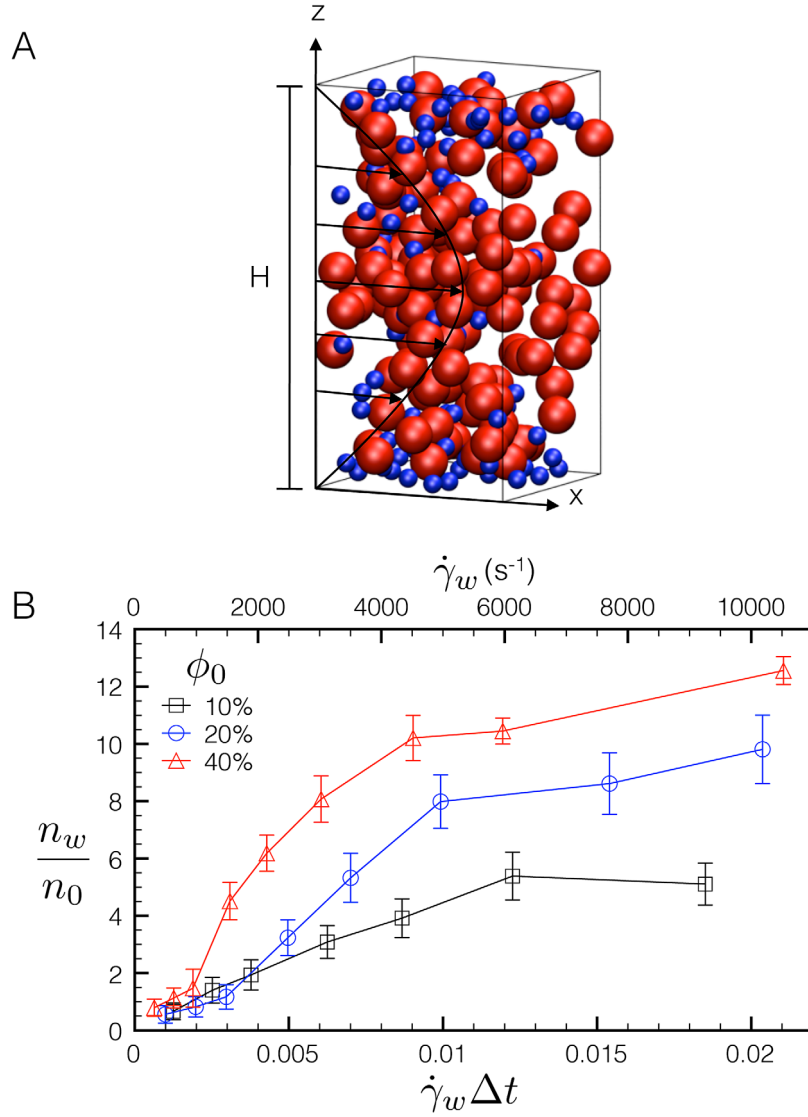
FIG. 4. (a) Representative snapshot of Lattice Boltzmann simulations of RBC-like colloids (large red beads) and platelet-like colloids (small blue beads) in pressure flow. (b) Mean near-wall excess of platelet-like colloids n_w/n_0 at different wall shear rate $\dot{\gamma}_w \Delta t$ with different volume fraction of RBC-like colloids ϕ_0. (See text for definition of symbols.)

and drug delivery.[79–82] Because of the large size and concentration differences, the concentration profile of platelets is mainly determined by RBCs. Eckstein and coworkers have established a drift-diffusion model for the platelet lateral motion:[51,52]

$$\frac{\partial n(z,t)}{\partial t} = \frac{\partial}{\partial z}\left(v_z(z)n(z,t) + D\frac{\partial n(z,t)}{\partial z} \right), \tag{1}$$

where $n(z,t)$ is the lateral platelet concentration, $v_z(z)$ a phenomenological drift function, and D a diffusion constant. Note that the diffusion constant D here is also determined by the platelet-RBC interaction and is usually 2 to 3 orders of magnitude higher than thermal diffusion.[51] In their original works, the drift term $v_z(z)$ is either assigned arbitrarily, or estimated backwards from the fully developed $n(z)$.[51,52] Here we derive $v_z(z)$ directly from physical reasoning similar to the shear-induced colloidal migration proposed by Leighton and Acrivos,[83] and Phillips and coworkers.[84] To our best knowledge, this is the first attempt to explicitly solve the drift function in the platelet margination problem. We first realize that due to the velocities increase
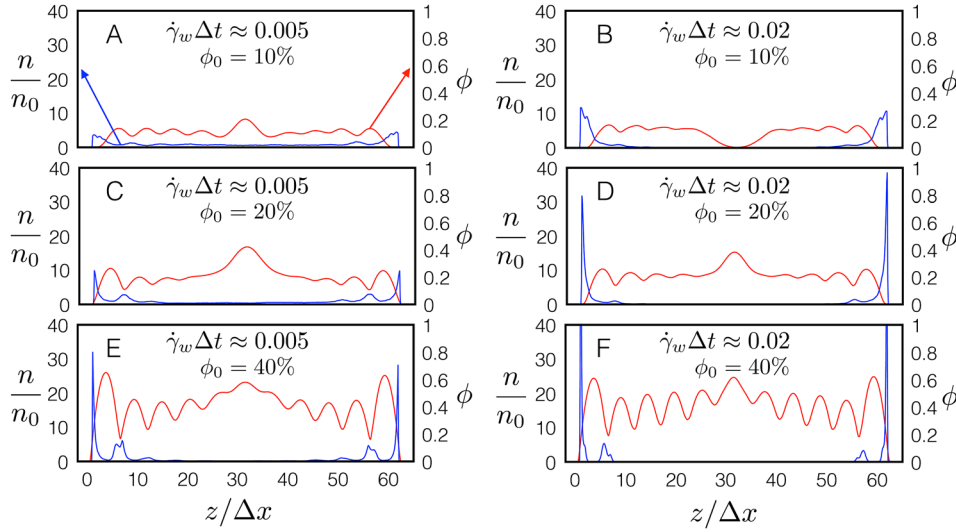
FIG. 5. Distribution of platelet-like colloids n/n_0 (blue curves) and RBC-like colloids ϕ (red curves) across the channel $z/\Delta x$ for (a) $\dot{\gamma}_w \Delta t \approx 0.005$ and $\phi_0 = 10\%$, (b) $\dot{\gamma}_w \Delta t \approx 0.02$ and $\phi_0 = 10\%$, (c) $\dot{\gamma}_w \Delta t \approx 0.005$ and $\phi_0 = 20\%$, (d) $\dot{\gamma}_w \Delta t \approx 0.02$ and $\phi_0 = 20\%$, (e) $\dot{\gamma}_w \Delta t \approx 0.005$ and $\phi_0 = 40\%$, and (f) $\dot{\gamma}_w \Delta t \approx 0.02$ and $\phi_0 = 40\%$ from LB simulations. (See text for definition of symbols.)

towards the center there are only two collision paths for the RBC and platelet pairs in shear flow: either a RBC approaches a platelet from slightly above, or a platelet approaches a RBC slight below (Fig. 6). Because the RBC sizes and concentrations are both considerably larger than the platelets, we can assume that the RBC distribution is not affected by the presence of platelets. If we further assume that the RBC and platelet interaction occurs predominantly through hydrodynamics, then a collision with RBCs will provide platelets with a velocity of $\sim \dot{\gamma}R$ or $-\dot{\gamma}R$ (where R is the effective radius of RBCs) depending on the specific collision paths (Fig. 6). The interaction probability is proportion to the volume fraction $\phi(z)$ at a specific height z. Assuming that the variance in the interaction probability over a distance of platelet size r is $r\frac{d}{dz}\phi$, we arrive at a drift velocity function for platelets:

$$v_z(z) = -\dot{\gamma}Rr\frac{d}{dz}\phi. \qquad (2)$$

To validate our theoretical approach, we perform SDE simulations of individual platelets (with uniform initial distribution) through[49,51]
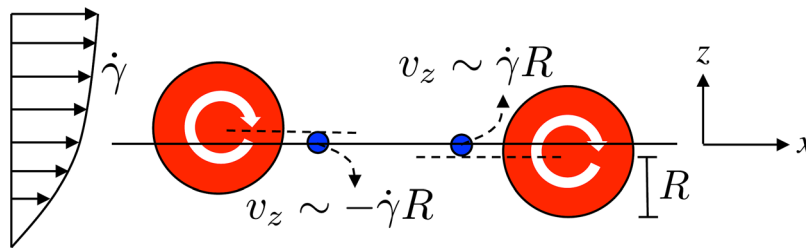
$$dz = v_z(z)dt + \xi_z(t), \qquad (3)$$

FIG. 6. Possible collision paths for a RBC and platelet pair in shear flow. Due to the velocities increase towards the center, there are only two collision paths for the RBC and platelet pairs in shear flow: either a RBC (large red sphere) approaches a platelet (small blue sphere) from slightly above (left illustration), or a platelet approaches a RBC slightly below (right illustration). If the interaction is mainly through hydrodynamics, for each collision the platelets acquire a velocity of $v_z \sim \dot{\gamma}R$ or $-\dot{\gamma}R$.

where z is the height of individual platelets, dt is an arbitrary time step, and $\xi_z(t)$ is a random walk such that $\xi_z(t)\xi_z(t') = 2D\delta(t - t')$. The drift term v_z is calculated directly from Eq. (2) with ϕ and $\dot{\gamma}$ extracted from Lattice Boltzmann simulations (Fig. 5). Figures 7(a) and 7(b) show the normalized drift term $v_z\Delta x/D$ (where Δx is a unit length) for selected $\dot{\gamma}_w\Delta t$ and ϕ_0. Note that the diffusion coefficient D is presumably also a function of z, as observed by Crowl and Folgelson.[49] However, for simplicity, we assume a constant D across the channel for given wall shear rates as suggested by Eckstein and coworkers.[49,51] With long enough time steps, the platelets in the SDE simulations reach a steady-state distribution. Figs. 7(c) and 7(d) show the platelet distribution n/n_0 calculated from SDE simulations with the drift term v_z given by Figs. 6(a) and 6(b). As shown, the near-wall excess of n/n_0 agrees particularly well with the results from explicit LB simulations (Fig. 5). In the present work, to solve v_z, the RBC distribution ϕ and fluid shear rate $\dot{\gamma}$ are extracted from our Lattice Boltzmann simulations. However, we believe the same result holds if we can measure ϕ and $\dot{\gamma}$ directly from experiments such as in Refs. 60 and 62. Knowing the exact drift function across the channel (which to the best of our knowledge has not been calculated before) provides us invaluable information not only for the platelet margination phenomenon, but also for the transportation of small particles across whole blood or other colloidal mixtures.

The platelet margination largely depends on the strong drift velocity adjacent to the wall regions (Figs. 7(a) and 7(b)) where both the shear rate $\dot{\gamma}(z)$ and the RBC collision gradient $\frac{d}{dz}\phi(z)$ are the highest. The highest shear rate near the walls comes from the parabolic-like flow profile, while the highest RBC collision gradient near the walls comes from the development of a RBC poor layer there, the so-called Fahraeus-Lindqvist effect.[85–87] A previous study has proposed a volume exclusion (or RBC crowding) description attributing the platelet margination to the more concentrated RBC distribution in the center,[88] and this point of view has later been extended with the inclusion of finite platelet sizes.[50] However, as has been pointed out by other studies,[49,89] this volume exclusion effect alone is probably insufficient to result in the inhomogeneous platelet distributions. Further, this description cannot explain the drastic increasing of the platelets near the walls at very high shear rates where the RBC distribution only changes marginally (Fig. 5).[84] In summary, we believe that both the non-homogeneous RBC distribution as well as the shear dependent hydrodynamic interactions are important to explain the transport towards and accumulation of platelet on the vessel wall.
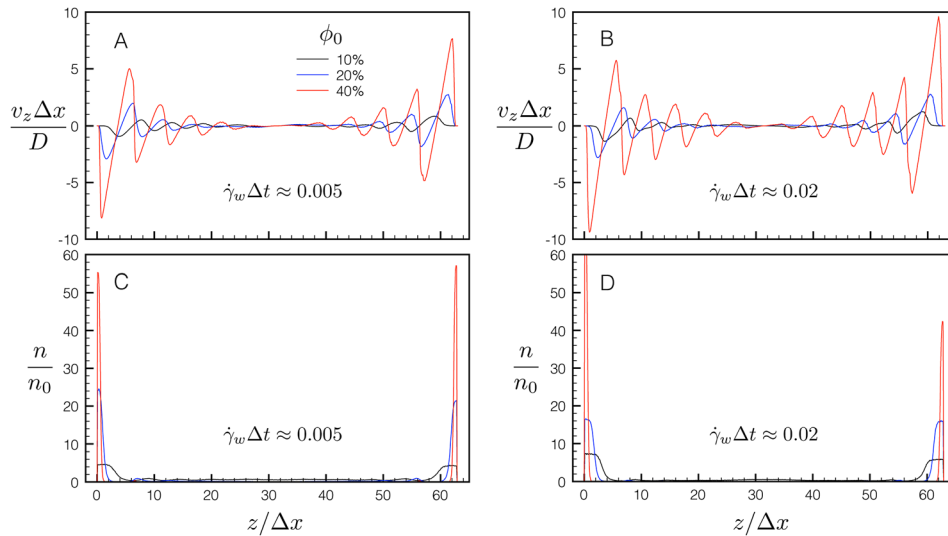

FIG. 7. (a) and (b) Theoretical drift velocities $v_z\Delta x/D$ for platelets calculated from Eq. (2) with RBC and shear rate distribution (ϕ and $\dot{\gamma}$) extracted from LB simulations. (c) and (d) Platelet distribution n/n_0 acquired from SDE simulations Eq. (3) with the drift velocities given by (a) and (b).

The convective-streaming mechanism proposed originally by Leighton and Acrivos,[83] perfected by Phillips and co-workers,[84] and refined by Eckstein[51] for platelets has a very simple analogy in the area of thermophoresis and Brownian motion when the diffusion constant is not homogeneous. If one thinks of a two-dimensional system undergoing Poiseuille flow and one moves in the frame of reference as a moving platelet, every time this platelet will "collide" with a rotating/threading RBC it will lead to platelet being stream up or down depending if the platelet is above the mid-plane of the RBC or below the mid plane respectively. The velocity with which the platelet will be convected up or down will depend on the rotational angular velocity (that is directly proportional to the local shear rate) and the size of the RBC. In Poiseuille flow, the shear rate is non-homogeneous, and this leads to random motion along the z axis with a gradient in effective/acquired vertical velocities. This translates directly to a gradient in the vertical effective diffusivity of the platelet, and we know that in such cases there appears a drift to regions with the higher diffusivities. In this case that corresponds to the region of largest shear rate which is near the boundary. To evaluate the total distribution, other factors need to be taken into account, such as the density of RBCs as a function of z since the fluxes depend on the average number of collisions. Above, we have derived the actual equation, but in this paragraph, we have just tried to give an intuitive meaning to the above derivation.

As a final point, it is important to mention that there are other processes that can take place in the margination process, as mentioned in the Introduction, but we believe they do not apply at high flow rates. First, given that the Re number is finite in this system, inertial effects will not be zero. However, the lift force from inertia scales with Re number ($Re \sim 10^{-2}$ at $\dot{\gamma} \sim 10\,000\,\mathrm{s}^{-1}$) and is about an order of magnitude smaller that the effects described here. Another important quantity that we need to discuss is related to the capillary number Ca. While Ca for RBCs at small shear rates is finite (order 0.01), at high flow rates the shape of the RBCs becomes fixed, the viscosity is lower, and thus the effective Ca increases very slightly to order 0.1–1 (even for large increases in shear rate[68]). A very important result, however, is that the angular velocity of real RBCs in the concentrated state has been measured to be independent of the Ca. The angular velocity (in units of $\dot{\gamma}$) is of order 0.3 across multiple orders of magnitude in Ca.[68] We actually model the $Ca = 0$ where the effect of surface tension becomes negligible by using non-deformable colloids. In this case, only the streaming of the platelets becomes the most important contribution to the lateral migration. Given the agreement between our numerical and theoretical results with the experiments we believe that this is the most important process at high flow rates in real RBC suspensions as well. Notice that the lift force from elastic stresses will be bounded at high flow rates because the change in deformation is negligible once the RBCs enter the tank-threading regime, and cannot explain the increase in margination at the elevated shear rates we study here.

CONCLUSION

This experimental and theoretical study provides quantitative evidence that the platelet adhesion to vWF is highly regulated by hematocrit level and flow rate. Furthermore, it is revealed that the origin of such behavior rests mainly in the distribution of platelets. We believe this finding is of importance in understanding the dependence of thrombus formation on hematocrit[30,31,74–78] and that it can lead to advances in the treatment of diseases associated with anomalous levels of red blood cells.[15] The lateral motion of platelets (or platelet-like particles) in flowing blood is formulated with a drift-diffusion model; in addition, the drift velocity is calculated unambiguously from the collision frequencies and hydrodynamic interactions between RBCs and platelets. This theoretical advance not only unveils the transport mechanism in complex hemodynamics,[16–21] but also has potential importance in drug delivery and drug distribution.[79–82]

ACKNOWLEDGMENTS

[1] S. P. Jackson, Blood **109**, 5087 (2007).
[2] Z. Ruggeri, J. Thromb. Haemostasis **1**, 1335 (2003).
[3] Z. Ruggeri, Nat. Med. **8**, 1227 (2002).
[4] Z. Ruggeri, J. Clin. Invest. **99**, 559 (1997).
[5] A. J. Reininger, Haemophilia **14**, 11 (2008).
[6] B. Furie and B. Furie, J. Clin. Invest. **115**, 3355 (2005).
[7] Z. Ruggeri, J. Clin. Invest. **105**, 699 (2000).
[8] J. Sadler, Annu Rev Biochem **67**, 395 (1998).
[9] D. Ginsburg and E. J. Bowie, Blood **79**, 2507 (1992); see http://bloodjournal.hematologylibrary.org/content/79/10/2507.
[10] Z. M. Ruggeri and T. S. Zimmerman, Blood **70**, 895 (1987); see http://bloodjournal.hematologylibrary.org/content/70/4/895.
[11] D. Provan, R. Stasi, A. C. Newland, V. S. Blanchette, P. Bolton-Maggs, J. B. Bussel, B. H. Chong, D. B. Cines, T. B. Gernsheimer, B. Godeau, J. Grainger, I. Greer, B. J. Hunt, P. A. Imbach, G. Lyons, R. McMillan, F. Rodeghiero, M. A. Sanz, M. Tarantino, S. Watson, J. Young, and D. J. Kuter, Blood **115**, 168 (2010).
[12] J. N. George, G. E. Raskob, S. R. Shah, M. A. Rizvi, S. A. Hamilton, S. Osborne, and T. Vondracek, Ann. Intern Med. **129**, 886 (1998).
[13] D. B. Cines, B. A. Konkle, and M. Furlan, Thromb. Haemostasis **84**, 528 (2000); see http://www.schattauer.de/en/magazine/subject-areas/journals-a-z/thrombosis-and-haemostasis/contents/archive/issue/890/manuscript/2541/show.html.
[14] G. G. Levy, W. C. Nichols, E. C. Lian, T. Foroud, J. N. McClintick, B. M. McGee, A. Y. Yang, D. R. Siemieniak, K. R. Stark, and R. Gruppo, Nature **413**, 488 (2001).
[15] B. Boneu and F. Fernandez, Transfus. Med. Rev. **1**, 182 (1987).
[16] W. S. Uijttewaal, E. J. Nijhof, P. J. Bronkhorst, E. Den Hartog, and R. M. Heethaar, Am. J. Physiol. Heart Circ. Physiol. **264**, H1239 (1993); see http://ajpheart.physiology.org/content/264/4/H1239.
[17] B. Woldhuis, G. J. Tangelder, D. W. Slaaf, and R. S. Reneman, Am. J. Physiol. Heart Circ. Physiol. **262**, H1217 (1992); see http://ajpheart.physiology.org/content/262/4/H1217.
[18] G. J. Tangelder, H. C. Teirlinck, D. W. Slaaf, and R. S. Reneman, Am. J. Physiol. Heart Circ. Physiol. **248**, H318 (1985); see http://ajpheart.physiology.org/content/248/3/H318.
[19] E. C. Eckstein, A. W. Tilles, and F. J. Millero, Microvasc. Res. **36**, 31 (1988).
[20] A. W. Tilles and E. C. Eckstein, Microvasc. Res. **33**, 211 (1987).
[21] C. Yeh and E. C. Eckstein, Biophys. J. **66**, 1706 (1994).
[22] B. Savage, E. Saldivar, and Z. Ruggeri, Cell **84**, 289 (1996).
[23] B. Savage, F. Almus-Jacobs, and Z. Ruggeri, Cell **94**, 657 (1998).
[24] A. Reininger, H. Heijnen, H. Schumann, H. Specht, W. Schramm, and Z. Ruggeri, Blood **107**, 3537 (2006).
[25] A. Curtis, J. Cell Biol. **20**, 199 (1964).
[26] A. Kloboucek, A. Behrisch, J. Faix, and E. Sackmann, Biophys. J. **77**, 2311 (1999).
[27] V. T. Turitto, H. J. Weiss, and H. R. Baumgartner, Microvasc. Res. **19**, 352 (1980).
[28] V. T. Turitto and H. R. Baumgartner, Microvasc. Res. **9**, 335 (1975).
[29] V. T. Turitto and H. J. Weiss, Ann. N. Y. Acad. Sci. **416**, 363 (1983).
[30] P. A. Aarts, P. A. Bolhuis, K. S. Sakariassen, R. M. Heethaar, and J. J. Sixma, Blood **62**, 214 (1983); see http://bloodjournal.hematologylibrary.org/content/62/1/214.
[31] V. T. Turitto and H. R. Baumgartner, ASAIO J. **21**, 593 (1975); see http://journals.lww.com/asaiojournal/Citation/1975/21000/Platelet_Deposition_on_Subendothelium_Exposed_to.79.aspx.
[32] B. Dünweg and A. J. C. Ladd, Adv. Polym. Sci. **221**, 89 (2009).
[33] C. Aidun, Y. Lu, and E. Ding, J. Fluid Mech. **373**, 287 (1998).
[34] A. Karnis, H. L. Goldsmith, and S. G. Mason, Nature **200**, 159 (1963).
[35] A. Karnis and S. G. Mason, J. Colloid Interface Sci. **24**, 164 (1967).
[36] P. Chan and L. G. Leal, J. Fluid Mech. **92**, 131 (1979).
[37] B. P. Ho and L. G. Leal, J. Fluid Mech. **65**, 365 (1974).
[38] S. Doddi and P. Bagchi, Phys. Rev. E **79**, 046318 (2009).
[39] C. W. Hsu and Y.-L. Chen, J. Chem. Phys. **133**, 034906 (2010).
[40] C. K. Aidun and J. R. Clausen, Annu. Rev. Fluid Mech. **42**, 439 (2010).
[41] J. R. Clausen and C. K. Aidun, Phys. Fluids **22**, 123302 (2010).
[42] A. Kumar and M. D. Graham, Soft Matter **8**, 10536 (2012).
[43] A. Kumar and M. Graham, Phys. Rev. Lett. **109**, 108102 (2012).
[44] A. Kumar and M. Graham, Phys. Rev. E **84**, 066316 (2011).
[45] H. Zhao and E. S. G. Shaqfeh, Phys. Rev. E **83**, 061924 (2011).
[46] H. Zhao, E. Shaqfeh, and V. Narsimhan, Phys. Fluids **24**, 011902 (2012).
[47] D. A. Reasor, Jr., M. Mehrabadi, D. N. Ku, and C. K. Aidun, Ann. Biomed. Eng. **41**, 238 (2013).
[48] L. M. Crowl and A. L. Fogelson, Int. J. Numer. Meth. Biomed. Eng. **26**, 471 (2010).
[49] L. Crowl and A. L. Fogelson, J. Fluid Mech. **676**, 348 (2011).
[50] A. A. Tokarev, A. A. Butylin, E. A. Ermakova, E. E. Shnol, G. P. Panasenko, and F. I. Ataullakhanov, Biophys. J. **101**, 1835 (2011).
[51] E. C. Eckstein and F. Belgacem, Biophys. J. **60**, 53 (1991).
[52] C. Yeh, A. C. Calvez, and E. C. Eckstein, Biophys. J. **67**, 1252 (1994).
[53] M. Lyon and L. Leal, J. Fluid Mech. **363**, 57 (1998).

[54]D. Semwogerere and E. Weeks, Phys. Fluids **20**, 043306 (2008).
[55]H. M. Vollebregt, R. Van der Sman, and R. M. Boom, Faraday Discuss. **158**, 89 (2012).
[56]H. Chen and A. Alexander-Katz, Phys. Rev. Lett. **107**, 128301 (2011).
[57]H. Chen, M. A. Fallah, V. Huck, J. I. Angerer, A. J. Reininger, S. W. Schneider, M. F. Schneider, and A. Alexander-Katz, Nature Commun. **4**, 1333 (2013).
[58]S. Dopheide, M. Maxwell, and S. Jackson, Blood **99**, 159 (2002).
[59]E. J. Lim, T. J. Ober, J. F. Edd, G. H. McKinley, and M. Toner, Lab Chip **12**, 2199 (2012).
[60]H. Fujiwara, T. Ishikawa, R. Lima, N. Matsuki, Y. Imai, H. Kaji, M. Nishizawa, and T. Yamaguchi, J. Biomech. **42**, 838 (2009).
[61]R. Lima, T. Ishikawa, Y. Imai, M. Takeda, S. Wada, and T. Yamaguchi, Ann. Biomed. Eng. **37**, 1546 (2009).
[62]R. Lima, T. Ishikawa, Y. Imai, M. Takeda, S. Wada, and T. Yamaguchi, J. Biomech. **41**, 2188 (2008).
[63]C. Migliorini, Y. Qian, H. Chen, E. B. Brown, R. K. Jain, and L. L. Munn, Biophys. J. **83**, 1834 (2002).
[64]C. Sun, C. Migliorini, and L. L. Munn, Biophys. J. **85**, 208 (2003).
[65]C. Sun and L. L. Munn, Biophys. J. **88**, 1635 (2005).
[66]L. L. Munn and M. M. Dupin, Ann. Biomed. Eng. **36**, 534 (2008).
[67]T. Fischer, Biophys. J. **93**, 2553 (2007).
[68]T. Krüger, M. Gross, D. Raabe, and F. Varnik, Soft Matter **9**, 9008 (2013).
[69]J. Skotheim and T. Secomb, Phys. Rev. Lett. **98**, 078301 (2007).
[70]J. M. Brader and M. Krüger, Mol. Phys. **109**, 1029 (2011).
[71]N. Schwierz and P. Nielaba, Phys. Rev. E **82**, 031401 (2010).
[72]K. Yeo and M. R. Maxey, Phys. Rev. E **81**, 051502 (2010).
[73]G. Segre and A. Silberberg, J. Fluid Mech. **14**, 136 (1962).
[74]V. T. Turitto, H. J. Weiss, and H. R. Baumgartner, J. Rheol. **23**, 735 (1979).
[75]E. F. Leonard, E. F. Grabowski, and V. T. Turitto, Ann. N. Y. Acad. Sci. **201**, 329 (1972).
[76]A. B. Strong, G. D. Stubley, G. Chang, and D. R. Absolom, J. Biomed. Mater. Res. **21**, 1039 (1987).
[77]A. A. Tokarev, A. A. Butylin, and F. I. Ataullakhanov, Biophys. J. **100**, 799 (2011).
[78]K. Konstantopoulos, S. Kukreti, and L. V. McIntire, Adv. Drug Deliver Rev. **33**, 141 (1998).
[79]S. Jadhav, C. D. Eggleton, and K. Konstantopoulos, Curr. Pharm. Des. **13**, 1511 (2007).
[80]P. Decuzzi, S. Lee, B. Bhushan, and M. Ferrari, Ann. Biomed. Eng. **33**, 179 (2005).
[81]P. Decuzzi, S. Lee, M. Decuzzi, and M. Ferrari, Ann. Biomed. Eng. **32**, 793 (2004).
[82]J. Tan, A. Thomas, and Y. Liu, Soft Matter **8**, 1934 (2012).
[83]D. Leighton and A. Acrivos, J. Fluid Mech. **181**, 415 (1987).
[84]R. J. Phillips, R. C. Armstrong, R. A. Brown, A. L. Graham, and J. R. Abbott, Phys. Fluids A **4**, 30 (1992).
[85]R. Fåhræus and T. Lindqvist, Am. J. Physiol. **96**, 562 (1931); see http://ajplegacy.physiology.org/content/96/3/562.
[86]R. H. Haynes, Am. J. Physiol. **198**, 1193 (1960); see http://ajplegacy.physiology.org/content/198/6/1193.
[87]A. R. Pries, D. Neuhaus, and P. Gaehtgens, Am. J. Physiol. **263**, H1770 (1992); see http://ajpheart.physiology.org/content/263/6/H1770.
[88]P. A. Aarts, S. A. Van Den Broek, G. W. Prins, G. D. Kuiken, J. J. Sixma, and R. M. Heethaar, Arterioscler., Thromb., Vasc. Biol. **8**, 819 (1988).
[89]J. F. Koleski and E. C. Eckstein, ASAIO Trans. **37**, 9 (1990); see http://journals.lww.com/asaiojournal/Citation/1991/01000/Near_Wall_Concentration_Profiles_of_1_0_and_2_5.4.aspx.